The Active Phase of Palladium during Methane Oxidation

ARTICLE *in* JOURNAL OF PHYSICAL CHEMISTRY LETTERS · FEBRUARY 2012

Impact Factor: 7.46 · DOI: 10.1021/jz300069s

THE JOURNAL OF PHYSICAL CHEMISTRY Letters

Letter

pubs.acs.org/JPCL

The Active Phase of Palladium during Methane Oxidation

A. Hellman,[†] A. Resta,[‡] N. M. Martin,[§] J. Gustafson,[§] A. Trinchero,[†] P.-A. Carlsson,[†] O. Balmes,[‡] R. Felici,[‡] R. van Rijn,[‡,∥] J. W. M. Frenken,[∥] J. N. Andersen,[§] E. Lundgren,[§] and H. Grönbeck*[,†]

[†]Competence Centre for Catalysis, Chalmers University of Technology, SE-412 96, Göteborg, Sweden

[‡]ESRF, 6 rue Jules Horowitz -38000 Grenoble, France

[§]Division of Synchrotron Radiation Research, Lund University, Box 118, SE-221 00, Sweden

[∥]Kamerlingh Onnes Laboratory, Leiden University, P.O. Box 9504, 2300 RA Leiden, The Netherlands

Supporting Information

ABSTRACT: The active phase of Pd during methane oxidation is a long-standing puzzle, which, if solved, could provide routes for design of improved catalysts. Here, density functional theory and in situ surface X-ray diffraction are used to identify and characterize atomic sites yielding high methane conversion. Calculations are performed for methane dissociation over a range of Pd and PdO_x surfaces and reveal facile dissociation on either under-coordinated Pd sites in PdO(101) or metallic surfaces. The experiments show unambiguously that high methane conversion requires sufficiently thick PdO(101) films or metallic Pd, in full agreement with the calculations. The established link between high activity and atomic structure enables rational design of improved catalysts.

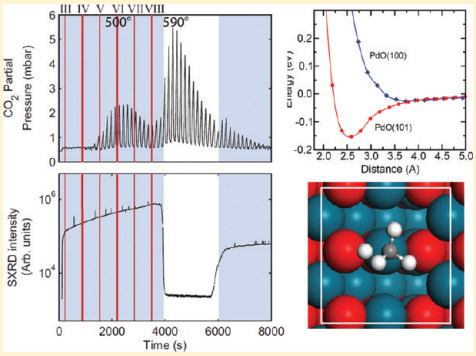

SECTION: Surfaces, Interfaces, Catalysis

A major challenge within heterogeneous catalysis is to determine the active phase during operating conditions. This is valid, in particular, for structurally ill-defined catalysts that are realized as metal particles dispersed on porous oxides. Nevertheless, it is structural information at the atomic scale that allow for catalyst development beyond trial-and-error approaches. One outstanding structural puzzle is the active phase of palladium during complete methane (CH_4) oxidation to water and carbon dioxide.[1] This is a key reaction when bio- or natural gas are combusted and there is currently a pressing need for catalysts with increased activity.

Different studies have attributed the high methane combustion activity of catalysts based on supported palladium to reduced (metallic) palladium,[2,3] metal supported surface oxides,[4] or bulk metal oxide.[1,5] As the exact composition of palladium oxide is difficult to measure, the latter phase is generally referred to as PdO_x instead of the stochiometric PdO. It has been noted that the CH_4 conversion rate over supported palladium is sensitive to catalyst dispersion and pretreatment conditions.[3] The difficulty to establish the active phase is clearly connected to the fact that the conversion rate, in the kinetic regime, is a consorted measure of the rate determining activation energy and the number of active sites (which may depend on operating conditions).

The structure and composition of palladium surfaces under oxidizing conditions have been studied intensively in the past and the surface oxides on Pd(100)[6] and Pd(111)[7] have been determined. On the basis of ab initio thermodynamics and scanning tunneling microscopy (STM), it has been suggested that the surface oxide on Pd(100) is present, or continuously reduced and reoxidized, during typical operating conditions for another oxidation reaction, namely, CO oxidation.[8−10] However, the role of the surface oxide during this reaction is still controversial,[11] and conclusions regarding the phase of the catalyst during CO oxidation could be obscured by the often observed bistability owing to kinetic phase transitions.[12]

From the diverging reports on the palladium catalyst for CH_4 oxidation it is obvious that the system has a complex behavior and that studies with high control over the Pd/PdO_x phase are needed. Herein, the active phase of Pd during CH_4 combustion is explored by density functional theory (DFT) calculations and in situ surface X-ray diffraction (SXRD) measurements. The results show that high methane conversion is obtained either on under-coordinated Pd-sites in PdO or on metallic Pd.

The DFT is used in a real space grid implementation[13,14] of the projector augmented wave (PAW) method.[15] The frozen core and projectors are generated with scalar relativistic corrections for Pd. Exchange and correlation contributions are described by the spin-polarized Perdew−Burke−Ernzerhof (PBE) functional.[16] Reciprocal space integration over the Brillouin zone is approximated with finite sampling. Activation energies are evaluated with the nudged-elastic band method[17] with at least 10 images between the initial and the final state.

Received: January 17, 2012
Accepted: February 19, 2012
Published: February 21, 2012

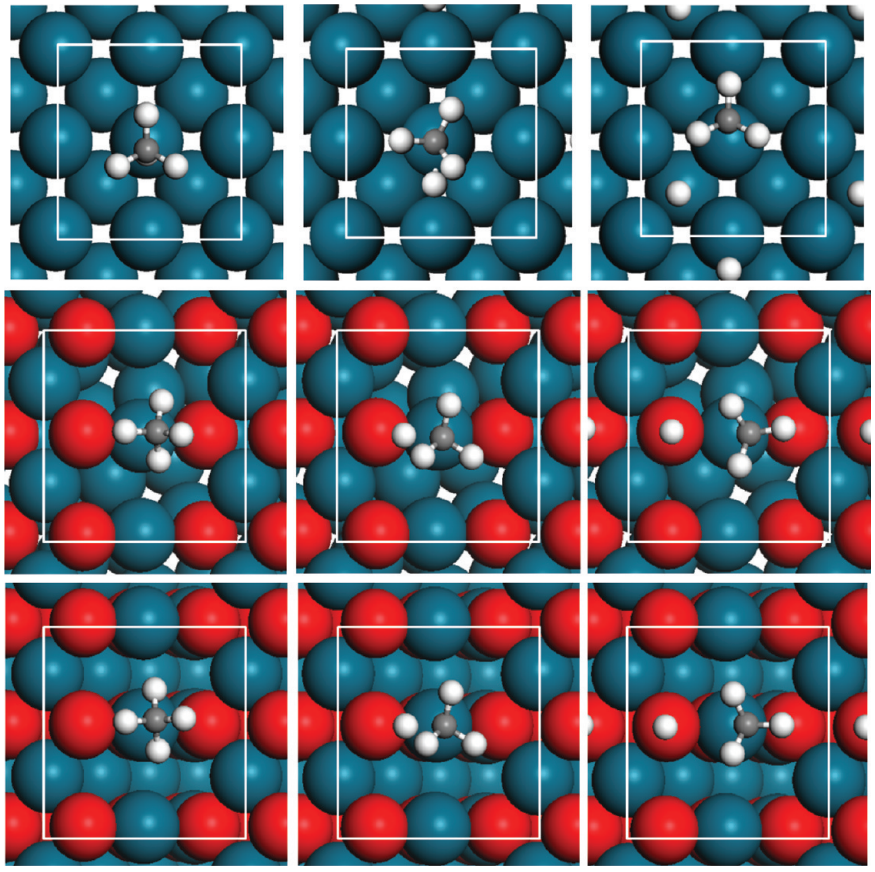

Figure 1. Atomic models of the (left to right) initial, transition, and final state structure for CH_4 dissociation on Pd(100) (top panels), $\sqrt{5}$ (mid panels), and PdO(101) (bottom panels). Atomic color codes: blue (Pd), red (O), gray (C), and white (H).

Table 1. Energetic and Structural Data for Hydrogen Abstraction over Palladium(-oxide) Surfaces[a]

	E_I	E_F	E_a	α_{H-C-H}
Pd(111)	0.00	0.42	0.86	109
Pd(100)	−0.03	0.35	0.73	109
Pd(211)	−0.02	0.23	0.56	110
PdO(100)	−0.02	−0.81	1.22	109
PdO(101)	−0.15	−0.57	0.50	114
$\sqrt{5}$	−0.02	0.38	1.22	110
$\sqrt{5}$-2 ML	−0.14	−0.55	0.51	114
$\sqrt{5}$-Pd(100)	−0.04	−0.93	0.98	110
PdO(100)-r	−0.04	−0.16	0.74	110
PdO(101)-r	−0.40	−0.57	0.40	117
$\sqrt{5}$-r	−0.07	−0.63	0.78	111

[a] E_I and E_F are the initial and final state energies with respect to CH_4 in the gas-phase, respectively. E_a is the activation energy for CH_4 dissociation. α_{H-C-H} is the H−C−H angle (°) for H atoms close to the surface. Energies are given in eV. $\sqrt{5}$-Pd(100) denotes a stripe of $\sqrt{5}$ on Pd(100), and "-r" denotes reduced forms of the oxide surfaces.

The SXRD experiments are performed at the ID03 beamline of the ESRF in Grenoble,[18,19] using a dedicated flow reaction setup.[20] The setup allows for ultrahigh vacuum (UHV) surface preparation techniques and SXRD measurements in gas composition environments close to realistic operating conditions. (For details see Supporting Information.)

Because of the high stability of methane and its weak interaction with surfaces, it can safely be assumed that the rate-determining step (RDS) in the catalytic cycle is methane dissociation.[21] The calculated activation energies for hydrogen abstraction over a range of surfaces are reported in Table 1 together with initial and final state energies, and an H−C−H angle. Three surfaces are considered for metallic Pd: (111), (100), and the stepped (211). For bulk oxide, we explore PdO(100), which is the most stable facet,[22] and PdO(101), which is the stable surface for an epitaxially grown PdO film on Pd(100).[23] In addition to the metal and oxide surfaces, the Pd(100)-($\sqrt{5} \times \sqrt{5}$)R27° surface oxide (hereafter denoted $\sqrt{5}$)[6] is studied (also with two monolayers, $\sqrt{5}$−2 ML), as well as reduced (oxygen deficient) forms of PdO(100), PdO(101), and $\sqrt{5}$. To model an oxide-metal interface, a stripe of a monolayer of PdO(101) on Pd(100) is investigated [$\sqrt{5}$-Pd(100)]. Structural models of selected surfaces are shown in Figure 1. (All structures are reported in the Supporting Information.)

The three metal surfaces are predicted to have activation energies in the range 0.55−0.85 eV; the highest is found for the close packed Pd(111), whereas the stepped Pd(211) has the lowest. The activation energy calculated for the stable stochiometric oxide surface PdO(100) is considerably higher, namely, 1.22 eV. PdO(101) is a corrugated surface with two types of Pd-sites: one coordinated to four oxygen atoms, which is the situation in the bulk and PdO(100), and one coordinated to only three oxygen atoms. The under-coordinated Pd atom has two oxygen neighbors in the surface plane and one in the second surface layer. Interestingly, hydrogen abstraction to form a methyl and an OH group proceeds with a barrier of only 0.50 eV at the under-coordinated Pd-site on PdO(101).[24,25] Even if $\sqrt{5}$ is constructed from a PdO(101) layer attached to

dx.doi.org/10.1021/jz300069s | J. Phys. Chem. Lett. 2012, 3, 678−682

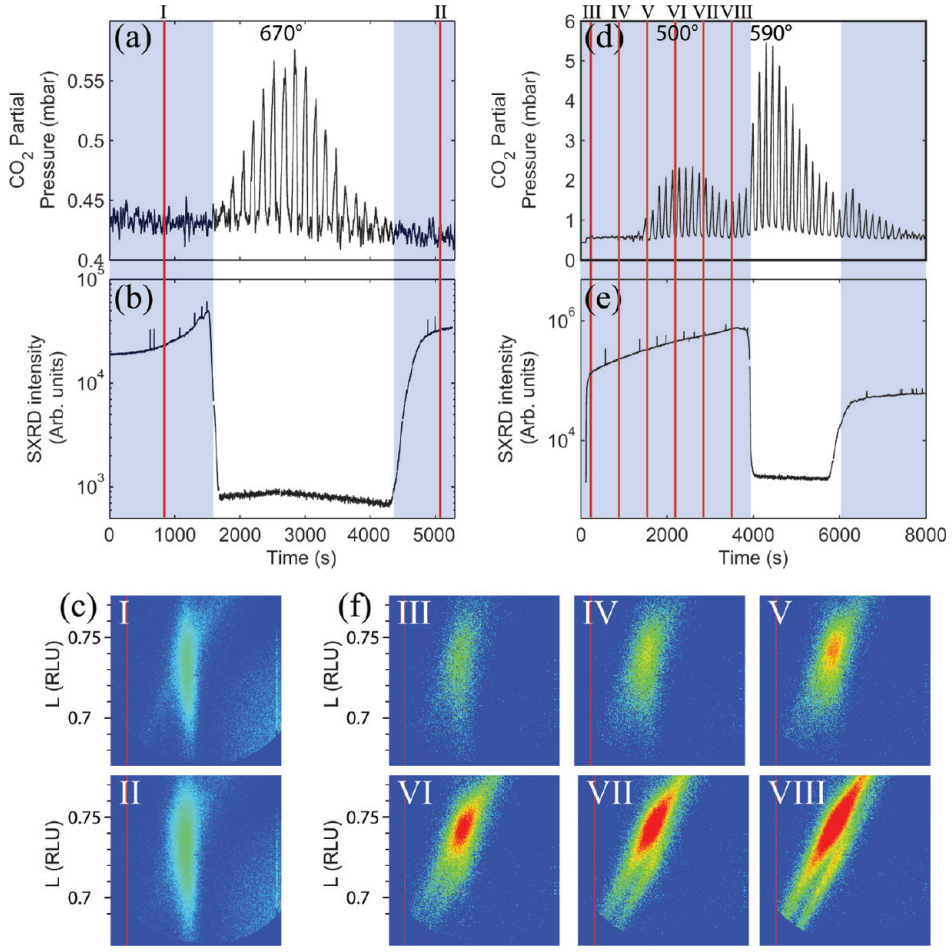

Figure 2. In situ SXRD experiments for Pd(100) during CH_4 combustion using 0.1 mbar CH_4 and 0.5 mbar O_2 (a–c) and 6 mbar CH_4 and 16 mbar O_2 (d,e), respectively. Both temperature ramps started and finished at 550 °C with the maximum temperature indicated. (a,d) CO_2 mass spectrometry signal. (b,e) Diffracted intensity from the PdO(101) planes. (c,f) 2D detector images corresponding to the temperatures as indicated by I–VII above. Note that the CO_2 production at low temperature in panel d stops increasing with temperature at the same time as the detector images indicate that the surface turns into powder.

Pd(100), the activation energy on the surface oxide is high (1.22 eV). The low PdO(101) barrier is, instead, retrieved in the case of two monolayers of Pd(101) on Pd(100).

As CH_4 oxidation consumes oxygen, partly reduced phases or surface oxides could, in principle, be of importance. Models of reduced forms of PdO(101), PdO(100), and $\sqrt{5}$ are constructed by removal of one oxygen atom in each surface cell. It should be noted that such processes are strongly endothermic.[26] The partial reduction of the oxide surfaces has a marked effect on the activation energies, which are lowered by ~0.5 eV for PdO(100) and $\sqrt{5}$. Reduction of the already active PdO(101), lowers the barrier by 0.1 eV. For CO oxidation, it has previously been suggested that edges of oxide phases could be of importance.[27] In order to explore such a system, half a monolayer of $\sqrt{5}$ has also been considered. On this surface, hydrogen abstraction occurs at the edge of the surface oxide with an activation energy of 1.05 eV, which is significantly higher than the value calculated for PdO(101).

We note that the dissociative adsorption of CH_4 is endothermic on the metal surfaces, whereas the products are stabilized when an OH group can be formed. However, even if the reaction products are stabilized by subsequent formation of OH groups, the presence of O on the metal surfaces increases the activation energy for hydrogen abstraction. The activation energy for CH_4 dissociation on Pd(100) with 0.25 coverage of O [p(2 × 2)] is calculated to be 1.01 eV.

In Figure 1, the structural models are shown for the initial, transition, and final states of CH_4 dissociation over Pd(100), $\sqrt{5}$, and PdO(101). CH_4 is on the metal surface adsorbed in a configuration where one H atom coordinates to a Pd atom. On $\sqrt{5}$ and PdO(101), the molecule bridges the under-coordinated Pd-atom. In all cases, the dissociation proceeds atop the Pd atom. On Pd(100), the final state is CH_3 adsorbed atop Pd and H in a 4-fold hollow position. For $\sqrt{5}$ and PdO(101), CH_4 dissociates into one OH and one CH_3 bonded to the under-coordinated Pd-atom.

The conclusions based on the computational findings are confirmed by in situ SXRD experiments combined with mass spectrometry, presented in Figure 2. The production of CO_2 is measured during linear temperature ramps (heating and cooling) with a common initial temperature of 350 °C. The results in Figure 2a–c correspond to partial pressures of 0.1 mbar CH_4 and 0.5 mbar O_2. The CO_2 production is minor below 550 °C and reaches a maximum at the highest temperature. The surface phase is initially identified by an elongation of the reflection in the L direction (see panel c), which is characteristic of the $\sqrt{5}$ surface oxide or a similar thin film.[28,29] There is a clear correlation between the onset of high

dx.doi.org/10.1021/jz300069s | J. Phys. Chem. Lett. 2012, 3, 678–682

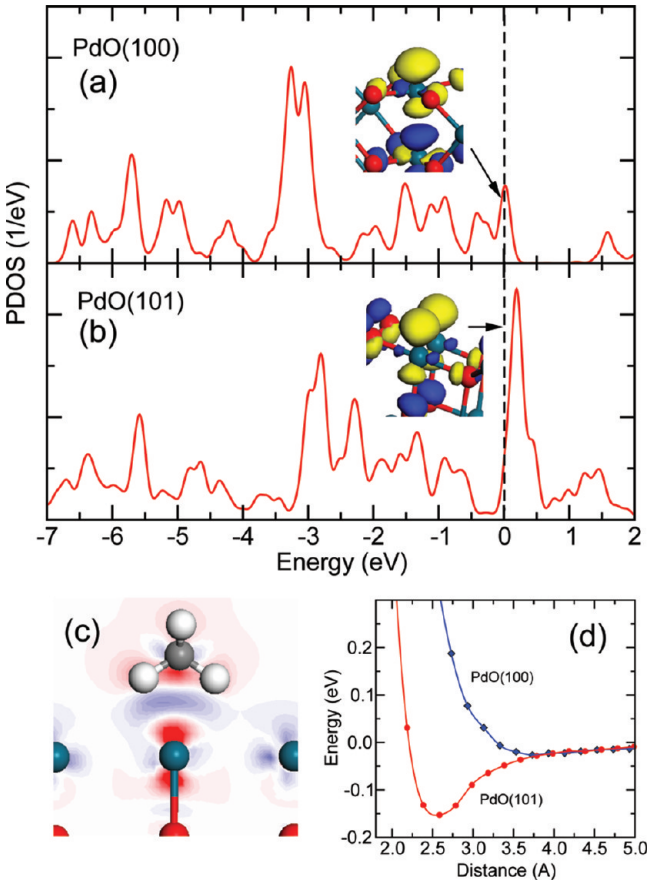

Figure 3. Partial density of states for (a) PdO(100) and (b) PdO(101). The insets show selected Kohn–Sham orbitals. (c) The charge density difference, $\rho(CH_4/PdO(101))-\rho(CH_4)-\rho(PdO(101))$, and (d) the PES for CH_4 over PdO(100) and PdO(101).

activity and decomposition of the surface oxide. During the cooling-ramp, the CO_2 production decreases with the temperature, and is close to zero at 480 °C. The diffraction signal of the thin oxide film reappears at approximately the same temperature. The experiment strongly suggests that the bare Pd metal or the metal with chemisorbed oxygen is more active for CH_4 combustion than the thin oxide phase.

A similar experiment with 6 mbar CH_4 and 16 mbar O_2 is shown in Figure 2d–f. Under these conditions, the surface is initially covered by a bulk-like PdO(101) film as evidenced by the spot-like feature in the detector image III (panel f), corresponding to the (101) reflection of PdO grown epitaxially on Pd(100) in the (101) direction.[28,29] In this experiment, the CO_2 production increases immediately as the temperature is ramped up to about 500 °C. Surprisingly, however, the activity drops upon further heating and does not recover until the surface turns metallic above 570 °C. This type of temperature dependence on the kinetics has been reported previously for Pd foils[30] and single crystals.[31]

The SXRD intensity in Figure 2d does not show any change that can explain the drop in activity at 500 °C. This can instead be done by inspection of the two-dimensional detector images in Figure 2f. As the temperature is raised, the epitaxial PdO film in image III grows thicker, as signaled by the stronger and sharper reflections in images IV and V. Upon further heating, however, the sharp spot turns into a powder diffraction ring. The powder ring becomes significant in image VI, which is recorded at the temperature when the activity does not increase despite further heating.

The data show that the lowest activation barrier is found for a sufficiently thick epitaxial PdO film. As such an epitaxial film is predicted to expose (101) facets,[23] this agrees well with the present calculations. Upon further heating, the surface breaks up, and the oxide loses its registry with the Pd(100) substrate. This leads to the exposure of the stable PdO surface, namely, PdO(100), which is calculated to have a high barrier for methane dissociation. The interpretation is consistent with the high-pressure X-ray photoelectron spectroscopy study in ref 31.

What is the reason for the difference in activity of the considered surface structures? If we first consider metallic Pd, it is clear that CH_4 interacts weakly with all surface orientations. However, the metallic sites have the ability to polarize CH_4 so as to facilitate the bond breaking once the C–H bond is stretched.[32] As for the PdO_x phases, the initial interaction of the bulk-like PdO(101)-facet stands out, with an adsorption energy of −0.15 eV (PdO(101), 2 ML-$\sqrt{5}$) and −0.4 eV (PdO(101)-r). Analysis of the H–C–H angle shows that methane in these systems is slightly activated. The presence of an activated molecule correlates with low reaction barriers. The barrier for hydrogen abstraction is a consequence of a crossing between the potential energy surfaces (PES) for C–H cleavage and the formation of chemisorbed surface species as discussed for hydrogen abstraction over metal complexes.[33,34] The results indicate that the repulsion in the entrance channel of the PES is reduced for the surfaces with low activation barrier. This is exemplified in Figure 3d, which shows the one-dimensional PES for methane approaching PdO(100) and PdO(101). CH_4 experiences a repulsive potential already at 3.2 Å on PdO(100), whereas the potential well is located at 2.55 Å on PdO(101).

To show the origin of the reduced repulsion, we report in Figure 3a,b the partial (5s) projected density of states (PDOS) for a metal atom in the surface layer of PdO(100) and the under-coordinated Pd atom in PdO(101). As the 5s states are the most diffuse metal states, sites with reduced 5s contributions in the occupied states are favorable for methane activation. For PdO(100), the PDOS is characterized by large 5s contributions in the occupied states close to the Fermi energy. On the other hand, for the under-coordinated Pd atom in PdO(101), a part of the 5s PDOS is instead shifted above the Fermi energy. Inspection of the unoccupied Kohn–Sham orbitals with s-character for PdO(101) (see insets) indicate that depopulation of this s-d hybrid should result in reduced repulsion. This detailed property of the electronic structure rationalizes the absence of a linear Brønsted–Evans–Polanyi relation between the activation energies and the final state energies for the oxides and is similar to the mechanism responsible for the high CO adsorption energy on PdO(101).[35] That the under-coordinated sites of PdO(101) are able to activate CH_4 is also visible in the charge density difference (3c), which clearly shows a polarization of the electronic charge in the molecule. Charge is depleted from the region between C and H and accumulated between H and the surface. The polarization of CH_4 over PdO(100) is negligible.

To conclude, the active phase of Pd for CH_4 combustion has been investigated by DFT calculations and in situ SXRD experiments. It is found that either under-coordinated Pd sites in PdO or metallic surfaces are required to obtain low activation energies for dissociative adsorption of CH_4, which is the rate-limiting step for this reaction. The results reconcile previous reports on the most active phase of Pd being either the

dx.doi.org/10.1021/jz300069s | J. Phys. Chem. Lett. 2012, 3, 678–682

metal[2,3] or the oxide,[1,5] and explains the anomalous temperature dependence of the activity at low-temperatures.[30,31] The identification and characterization of active sites for hydrogen abstraction over PdO provides handles for rational design of oxide-based catalysts for methane oxidation.

■ ASSOCIATED CONTENT

Supporting Information

Details of the computational and experimental methods, structural models of all investigated structures, and results from the microkinetic simulations. This material is available free of charge via the Internet at http://pubs.acs.org.

■ AUTHOR INFORMATION

Corresponding Author

*E-mail: ghj@chalmers.se.

Notes

The authors declare no competing financial interest.

■ ACKNOWLEDGMENTS

Support from the Swedish Foundation for Strategic Research, the Knut and Alice Wallenberg Foundation, and the Swedish Research Council is gratefully acknowledged. The calculations were performed at PDC (Stockholm). We thank the technical staff of the ID03 beamline, in particular T. Dufrane, for continuous support during the experiments. A.H. and H.G. acknowledge fruitful discussions with A. Asthagiri.

■ REFERENCES

(1) Burch, R.; Loader, P. K.; Urbano, F. J. *Catal. Today* **1996**, *27*, 243.
(2) Hicks, R. F.; Qi, H. H.; Young, M. L.; Lee, R. G. *J. Catal.* **1990**, *122*, 280.
(3) Lyubovsky, M.; Pfefferle, L. *Catal. Today* **1999**, *47*, 29.
(4) Oh, S.; Mitchell, P. J.; Siewert, R. *J. Catal.* **1991**, *123*, 287.
(5) McCarthy, J. G. *Catal. Today* **1995**, *26*, 283.
(6) Kostelnik, P.; Seriani, N.; Kresse, G.; Mikkelsen, A.; Lundgren, E.; Blum, V.; Sikola, T.; Varga, P.; Schmid, M. *Surf. Sci.* **2007**, *601*, 1574.
(7) Lundgren, E.; Kresse, G.; Klein, C.; Borg, M.; Andersen, J. N.; DeSantis, M.; Gauthier, Y.; Schmid, M.; Varga, P. *Phys. Rev. Lett.* **2002**, *88*, 246103.
(8) Rogal, J.; Reuter, K.; Scheffler, M. *Phys. Rev. Lett.* **2007**, *98*, 046101.
(9) Rogal, J.; Reuter, K.; Scheffler, M. *Phys. Rev. B* **2007**, *75*, 205433.
(10) Hendriksen, B. L. M.; Babaru, S. C.; Frenken, J. W. M. *Surf. Sci.* **2004**, *552*, 229.
(11) Gao, F.; McClure, S. M.; Cai, Y.; Gath, K. K.; Wang, Y.; Chen, M. S.; Guo, Q. L.; Goodman, D. W. *Surf. Sci.* **2009**, *603*, 65.
(12) Zhdanov, V. P.; Kasemo, B. *Surf. Sci. Rep.* **1994**, *20*, 111.
(13) Mortensen, J. J.; Hansen, L. B.; Jacobsen, K. W. *Phys. Rev. B* **2005**, *71*, 035109.
(14) https://wiki.fysik.dtu.dk/gpaw; accessed August 11, 2010.
(15) Blochl, P. E. *Phys. Rev. B* **1994**, *50*, 17953.
(16) Perdew, J. P.; Burke, K.; Ernzerhof, M. *Phys. Rev. Lett.* **1996**, *77*, 3865.
(17) Henkelman, G.; Uberuaga, B. P.; Jonsson, H. *J. Chem. Phys.* **2000**, *113*, 9901.
(18) Ferrer, S.; Comin, F. *Rev. Sci. Instrum.* **1995**, *66*, 1674.
(19) Balmes, O.; van Rijn, R.; Wermeille, D.; Resta, A.; Petit, L.; Isern, H.; Dufrane, T.; Felici, R. *Catal. Today* **2009**, *145*, 220.
(20) van Rijn, R.; Ackermann, M. D.; Balmes, O.; Dufrane, T.; Geluk, A.; Gonzalez, H.; Isern, H.; de Kuyper, E.; Petit, L.; Sole, V. A.; Wermeille, D.; Felici, R.; Frenken, J.W. M. *Rev. Sci. Instrum.* **2010**, *81*, 014101.
(21) The assumption that dissociation of the first H atom is the RDS is consistent with experiments on supported catalysts, which show that the reaction order is one with respect to CH_4 pressure. Previous DFT calculations indicate that the initial dissociation has the highest activation energy in the complete transformation of CH_4 to elemental C and H on Pd(100).[36] By use of a microkinetic model, in which two different RDSs are explored (CH_4 dissociation or water formation) CH_4 dissociation is shown to be the RDS at all relevant reaction conditions. See Supporting Information.
(22) Rogal, J.; Reuter, K.; Scheffler, M. *Phys. Rev. B* **2004**, *69*, 075421.
(23) Seriani, N.; Harl, J.; Mittendorfer, F.; Kresse, G. *J. Chem. Phys.* **2009**, *131*, 054701.
(24) Weaver, J. F.; Hakanoglu, C.; Hawkins, J. M.; Asthagiri, A. *J. Chem. Phys.* **2010**, *132*, 024709.
(25) Kinnunen, N. M.; Hirvi, J. T.; Suvanto, M.; Pakkanen, T. A. *J. Phys. Chem. C* **2011**, *39*, 19197.
(26) With respect to gas phase O_2, the energy penalty is 1.92 and 1.94 eV for PdO(100) and PdO(101), respectively.
(27) Westerström, R.; Wang, J. G.; Ackerman, M. D.; Gustafson, J.; Resta, A.; Mikkelsen, A.; Andersen, J. N.; Lundgren, E.; Balmes, O.; Torrelles, X.; Frenken, J. W. M.; Hammer, B. *J. Phys.: Condens. Matter* **2008**, *20*, 184018.
(28) Lundgren, E.; Gustafson, J.; Mikkelsen, A.; Andersen, J.; Stierle, A.; Dosch, H.; Todor-ova, M.; Rogal, J.; Reuter, K.; Scheffler, M. *Phys. Rev. Lett.* **2004**, *92*, 046101.
(29) Balmes, O.; Resta, A.; Wermeille, D.; Westerström, R.; Gustafson, J.; Felici, R.; Lund-gren, E.; Frenken, J. W. M. *Phys. Chem. Chem. Phys.* **2011**, *13*, 13167.
(30) Salomonsson, P.; Johansson, S.; Kasemo, B. *Catal. Lett.* **2011**, *33*, 1.
(31) Gabasch, H.; Hayek, K.; Kloetzer, B.; Unterberger, W.; Kleimenov, E.; Teschner, D.; Zafeiratos, S.; Haevecker, M.; Knop-Gericke, A.; Schloegl, R.; Aszalos-Kiss, B.; Zemlyanov, D. *J. Phys. Chem. C* **2007**, *111*, 7957.
(32) Bengaard, H. S.; Alstrup, I.; Chorkendorff, I.; Ullmann, S.; Rostrup-Nielsen, J. R.; Norskov, J. K. *J. Catal.* **1999**, *187*, 238.
(33) Blomberg, M. R. A.; Siegbahn, P. E. M.; Svensson, M. *J. Am. Chem. Soc.* **1992**, *114*, 6095.
(34) Balcells, D.; Clot, E.; Eisenstein, O. *Chem. Rev.* **2010**, *110*, 749.
(35) Zorn, K.; Giorgio, S.; Halwax, E.; Henry, C. R.; Grönbeck, H.; Rupprechter, G. *J. Phys. Chem. C* **2011**, *115*, 1103.
(36) Zhang, C. J.; Hu, P. *J. Chem. Phys.* **2002**, *116*, 322.